

An unlikely route to low lattice thermal conductivity: small atoms in a simple layered structure

Wanyue Peng ^a, Guido Petretto ^b, Gian-Marco Rignanese ^b,
Geoffroy Hautier ^b, Alexandra Zevalkink ^a

Abstract—In the design of materials with low lattice thermal conductivity, compounds with high density, low speed of sound, and complexity at either the atomic, nano- or microstructural level are preferred. The layered compound Mg_3Sb_2 defies these prevailing paradigms, exhibiting lattice thermal conductivity comparable to PbTe and Bi_2Te_3 , despite its low density and simple structure. The excellent thermoelectric performance ($zT \sim 1.5$) in n -type Mg_3Sb_2 has thus far been attributed to its multi-valley conduction band, while its anomalous thermal properties have been largely overlooked. To explain the origin of the low lattice thermal conductivity of Mg_3Sb_2 , we have used both experimental methods and ab initio phonon calculations to investigate trends in the elasticity, thermal expansion and anharmonicity of $A\text{Mg}_2\text{Pn}_2$ Zintl compounds with $A = \text{Mg}, \text{Ca}, \text{Yb}$, and $\text{Pn} = \text{Sb}$ and Bi . Phonon calculations within the quasi-harmonic approximation reveal large mode Grüneisen parameters in Mg_3Sb_2 compared with isostructural compounds, in particular in transverse acoustic modes involving shearing of adjacent anionic layers. Measurements of the elastic moduli and sound velocity as a function of temperature using resonant ultrasound spectroscopy provide a window into the softening of the acoustic branches at high temperature, confirming their exceptionally high anharmonicity. We attribute the anomalous thermal behavior of Mg_3Sb_2 to the diminutive size of Mg , which may be too small for the octahedrally-coordinated site, leading to weak, unstable interlayer Mg - Sb bonding. This suggests more broadly that soft shear modes resulting from undersized cations provide a potential route to achieving low lattice thermal conductivity low-density, earth-abundant materials.

I. INTRODUCTION

The ability to predict and design thermal transport in bulk materials is a fundamental requirement in a wide range of applications. In areas such as the

development of thermal barrier coatings and thermoelectric materials, engineering materials with extremely low lattice thermal conductivity, κ_L , is vital. In materials with inherently high thermal conductivity (e.g., Si), low κ_L can be achieved using clever microstructural design, nanostructuring, defects, or alloying to scatter phonons [5], [7], [25]. Alternatively, inherently low κ_L can be achieved in compounds with either low phonon velocities or high rates of phonon-phonon Umklapp scattering. Thus, in the search for materials with low κ_L , compounds with high density (PbTe , Bi_2Te_3), soft bonds, and complex atomic structures (e.g., $\text{Yb}_{14}\text{MnSb}_{11}$ with 104 atoms per unit cell [57]) are favored, since these features lead to low phonon velocities [58]. Design parameters for achieving high rates of phonon-phonon scattering (i.e., materials with large Grüneisen parameters) are more elusive, although a number of studies have recently provided guidance here as well. For example, highly anharmonic phonon modes arise from soft or unstable bonds (e.g., associated with Cu lone pairs, rattlers in cage compounds, resonance bonding, etc. [29], [33], [28]) and they generally emerge in the vicinity of lattice instabilities [2], [10].

The binary compound, Mg_3Sb_2 , which crystallizes in the layered CaAl_2Si_2 structure type, appears to defy standard paradigms used to identify materials with low lattice thermal conductivity. Mg_3Sb_2 has a low density, relatively high speed of sound, and a simple atomic structure with only five atoms per primitive cell, yet despite having roughly half the density of PbTe and Bi_2Te_3 , it has comparable κ_L at room temperature (1-1.5 W/mK [4], [54], [51]). As illustrated by Fig. 2a, the low κ_L of Mg_3Sb_2 is anomalous compared with other $A\text{M}_2\text{X}_2$ compounds with the CaAl_2Si_2

^a Michigan State University, East Lansing, MI, USA.

^b Université catholique de Louvain, Louvain-la-Neuve, Belgium

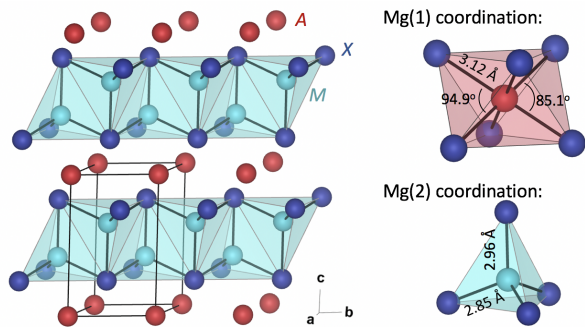


Fig. 1. Mg_3Sb_2 crystallizes in the CaAl_2Si_2 structure (space group $P\bar{3}m1$), characterized by anionic M_2X_2 slabs separated by A cations. In the binary compounds Mg_3Sb_2 and Mg_3Bi_2 , the Mg(1) occupies the octahedrally-coordinated A site and Mg(2) the tetrahedrally-coordinated M site [34].

structure type. Although Mg_3Sb_2 is one of the lightest compounds in the series, it exhibits one of the lowest values of κ_L . In particular, we note that the reported κ_L of Mg_3Sb_2 is much lower than that of CaMg_2Sb_2 [cite Max], which differs only by the presence of Ca instead of Mg on the octahedral site.

AM_2X_2 compounds with the CaAl_2Si_2 structure have attracted a great deal of interest for thermoelectric applications [49], [41] owing to the chemical diversity and flexibility in tuning transport properties. Most commonly, A is divalent cation such as Mg, Ca, Yb, Eu, M is a divalent metal such as Mg, Mn, Zn, or Cd, and X is a pnictogen species. Shown in Figure 1, the structure of CaAl_2Si_2 is composed of 2-dimensional anionic M_2X_2 slabs in which M is tetrahedrally coordinated by X [6]. The cations occupying the layers between the anion slabs are octahedrally coordinated by X . In the binary members of this structure (e.g., Mg_3Sb_2 and Mg_3Bi_2), the Mg(1) occupies the octahedral M site and Mg(2) the tetrahedral A site, and exhibits significantly different bond length at each site.

Recently, excellent thermoelectric performance has been demonstrated in n -type Mg_3Sb_2 -based samples, with zT up to 1.6 reported by several independent groups [55], [65], [66], [21], [50]. This surpasses all previous results for isostructural compounds, all of which have been p -type. To date, experimental and theoretical investigations of Mg_3Sb_2 have focused on the electronic properties; e.g., the defect origin of n -type doping [39], [55],

the multi-valley character of the conduction band [65], [23], [48], [21], and routes to increased carrier mobility [27], [50]. In contrast, the anomalously low κ_L of both n - and p -type Mg_3Sb_2 has not been investigated, though it plays an equally important role in leading to the high zT . The aim of the present study is to shed light on the origins of low lattice thermal conductivity in Mg_3Sb_2 . We employ experimental methods and ab initio phonon calculations to investigate trends in the thermal properties of binary and ternary AMg_2Pn_2 compounds with $A = \text{Mg}, \text{Ca}, \text{Yb}$, and $Pn = \text{As}, \text{Sb}$ and Bi , revealing previously unrecognized soft shearing modes and highly anharmonic acoustic phonons in Mg_3Sb_2 . This work shows that the soft shear modes resulting from undersized cations provide a potential route to achieving low lattice thermal conductivity in simple, low-density structures.

II. METHODS

A. Synthesis

AMg_2Pn_2 compounds with $A = \text{Mg}, \text{Ca}, \text{Yb}$ and $Pn = \text{Sb}, \text{Bi}$ were synthesized by direct ball-milling of the elements followed by spark plasma sintering. The corresponding stoichiometric elements (99.8% Mg shot, 99.5% Ca shot, 99.9% Yb chunk, 99.99% Sb from Alfa Aesar and 99.99% Rotometal Bi) were cut into small pieces in an argon filled glovebox, loaded into stainless steel vials with two 10 mm diameter stainless balls, and milled for one hour using a SPEX mill. The powder was then loaded into graphite dies with 10 mm bores and sintered using the profile shown in Table I under a pressure of 31 MPa using a Dr. Sinter SPS-211LX. The pressure was removed immediately when cooling started. The densities of all the samples were obtained by measurement of mass and geometry. All samples were at least 97% of the theoretical density. Phase purity was confirmed using a Rigaku X-ray Diffraction system, showing that samples contained less than 3% of secondary phases.

B. Characterization

The temperature-dependent elastic moduli of all compositions were measured by resonant ultrasound spectroscopy (RUS) [32], [1] using a custom

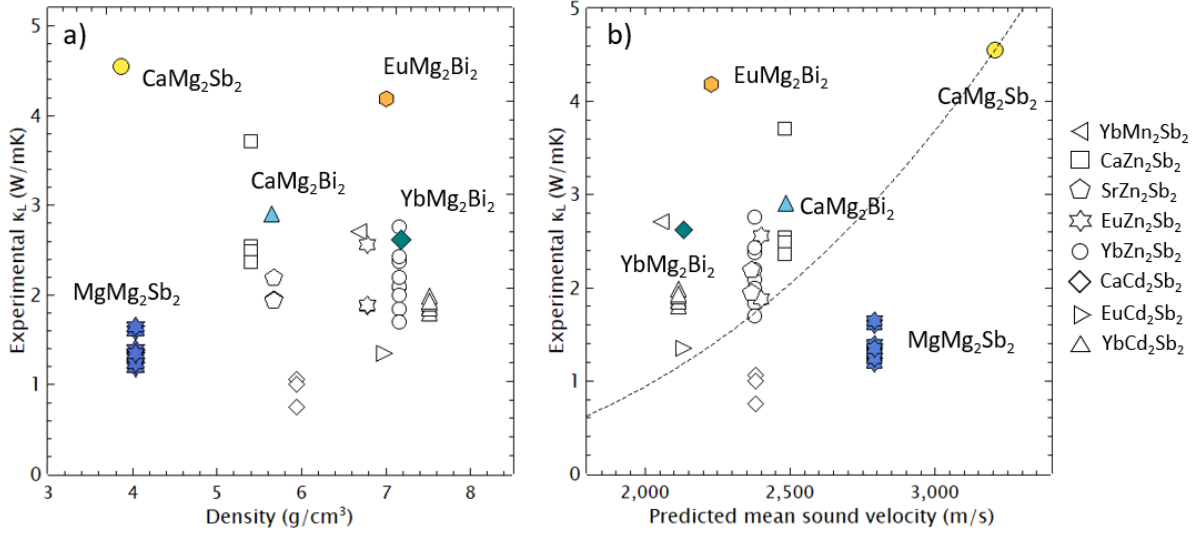


Fig. 2. The experimental lattice thermal conductivity, κ_L , of Mg_3Sb_2 is significantly lower than isostructural AMg_2X_2 compounds with similar a) density and b) predicted speed of sound (κ_L data can be found in Ref. [41]). The mean speed of sound, v_s , was estimated using the calculated elastic moduli from MaterialsProject.org and experimental densities [8], [9]. The dashed line shows a $\kappa_L \propto v_s^3$ dependence as a guide to the eye. Compounds with $M = \text{Mg}$ are shown in color, as these are the primary focus of the current study.

TABLE I

MAXIMUM TEMPERATURE AND HOLD TIME USED DURING SPARK PLASMA SINTERING OF AMg_2Pn_2 ($A=\text{Mg, CA, YB}$ AND $\text{Pn}=\text{SB, BI}$) SAMPLES.

	Mg_3Sb_2	CaMg_2Sb_2	YbMg_2Sb_2
Temp. ($^{\circ}\text{C}$)	850	650	650
Time (min)	15	10	10
	Mg_3Bi_2	CaMg_2Bi_2	YbMg_2Bi_2
Temp. ($^{\circ}\text{C}$)	600	700	700
Time (min)	10	10	15

modification of a Mangalux-RUS Quasar 4000 system in a furnace with a flowing Ar atmosphere. Cylindrical samples were mounted on a tripod transducer setup. One transducer induced the mechanical vibrations and the remaining two detected the specimen resonances. The elastic moduli were measured in 20 K intervals from 303 K up to 673 K. The sinusoidal driving frequency was swept from 0 to 500 kHz. The RUS measurement at each temperature was typically completed within one minute. Data was analyzed using commercial Quasar2000 CylModel software to match predicted and observed resonant frequencies.

Thermal expansion of all compositions was measured from 303 K to 573 K using a Rigaku Smartlab XRD equipped with a high-temperature stage. The samples were ground into fine powders

that were then placed on a graphite foil on top of a platinum tray. The measurements were performed under vacuum to prevent oxidation. The thermocouple goes into the inner part of the platinum tray to increase the accuracy of the temperature measurement. The heating rate is 10 K/min with a 1 min hold and sample height alignments were performed before each measurement to account for the combined thermal expansion of the holder and sample.

C. Calculation details

The ABINIT software package[14], [13], [62] was used to perform density functional theory (DFT) and density functional perturbation theory (DFPT) simulations to obtain phonon properties and elastic constants [3], [12], [15], [18]. The exchange-correlation functional was described using the PBEsol[42] approximation, that has proven to provide accurate phonon frequencies compared to experimental data[19]. Norm-conserving pseudopotentials[17] extracted from the Pseudo-Dojo pseudopotentials table version 0.3[61] were used for all the elements and the Brillouin zone was sampled with $8 \times 8 \times 5$ Monkhorst-Pack grids [35], [43]. Due to standard DFT's known limitations in describing the band gap, we limit our analysis to Mg_3Sb_2 , CaMg_2Sb_2 and CaMg_2Bi_2 ,

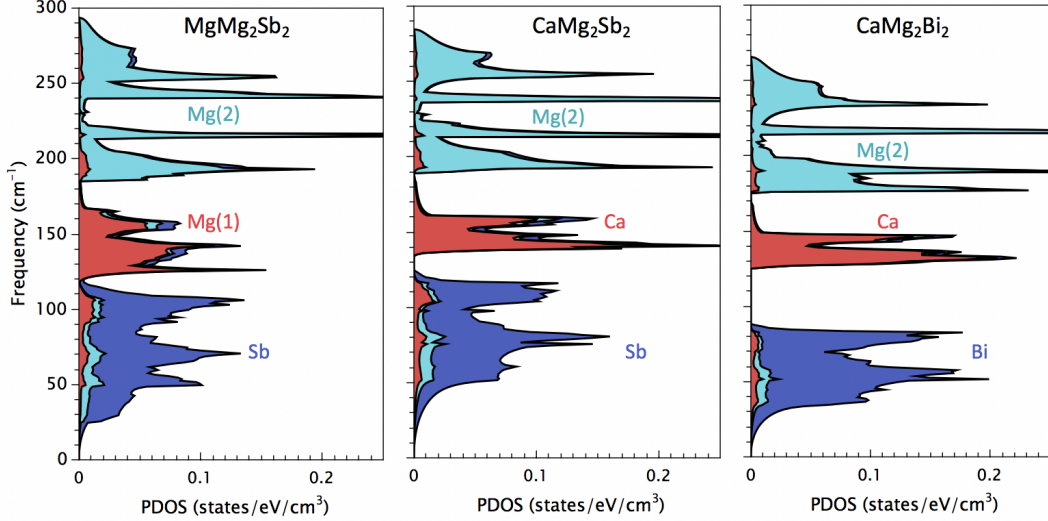


Fig. 3. The atom-projected phonon density of states of Mg_3Sb_2 , CaMg_2Sb_2 and CaMg_2Bi_2 shows that the low-, mid-, and high- frequency regimes are dominated, respectively, by displacements of the anions (Sb, Bi), cations (Mg(1), Ca), and metal site (Mg(2)). The species on the cation site (Mg or Ca) does not strongly influence the maximum frequency or the average phonon velocities.

for which the electronic structures are correctly described in our approximations. Temperature-dependent thermal expansion data was extracted from the phonon dispersion by relaxing the position of the atoms and shape of the unit cell at different fixed volumes in the framework of the quasiharmonic approximation. Once extracted the thermal expansion coefficient, the Young’s modulus, Y , was calculated as a function of temperature by using the corresponding unit cell volume, from which 300 K was chosen as the initial point Y_0 . Grüneisen parameters were obtained as the derivative of the phonon frequencies with respect to the volume.

III. RESULTS AND DISCUSSION

A. Anomalously low lattice thermal conductivity in Mg_3Sb_2

Inherently low lattice thermal conductivity, κ_L , stems from either slow phonon velocities, v , or short phonon relaxation times, τ [53], [58]. Of these two factors, the phonon velocities are the more accessible quantity; they can either be estimated roughly using the speed of sound, or they can be obtained from the calculated or measured phonon dispersion. Thus, in investigating the origin of low κ_L in any material, we should always begin by asking whether or not low phonon velocity is responsible. In Figure 2b, we have plotted

the experimental κ_L of AM_2X_2 compounds as a function of the predicted mean speed of sound, v_s . We have only included data from unalloyed samples, most of which exhibit the $1/T$ temperature dependence expected for Umklapp scattering dominated transport. Due to the lack of experimental speed of sound data in most of the compounds, we used the calculated bulk and shear elastic moduli from Materials Project to estimate v_s [9] (details can be found in S.I. section 1). A comparison of the experimental and computed speed of sound in the compounds in this study show less than 7% difference, showing the reliability of this approach.

When thermal transport is limited by Umklapp phonon-phonon scattering, κ_L can be approximated as proportional to v_s^3/γ^2 , where γ is the Grüneisen parameter [53], [58], [64]. The dashed curve in Figure 2b has a v_s^3 dependence, provided as a “guide to the eye” to show that the low κ_L of Mg_3Sb_2 cannot be explained by taking into account the sound velocity. This implies either a) that additional scattering sources are present and unique to Mg_3Sb_2 samples, b) that the Grüneisen parameter of Mg_3Sb_2 is abnormally large, leading to increased Umklapp scattering or c) that the sound velocity fails to capture broader trends in the phonon group velocities in this structure type. We note that there is currently no evidence that the microstructure or defect concentrations in Mg_3Sb_2

samples differ strongly from other AM_2X_2 samples. Similar values for κ_L reported from multiple research groups and processing approaches lead us to believe that low κ_L is an inherent characteristic of Mg_3Sb_2 [4], [66], [54], [51], [50], [39]. Thus, in the current investigation, we focus on the latter two inherent explanations for low κ_L .

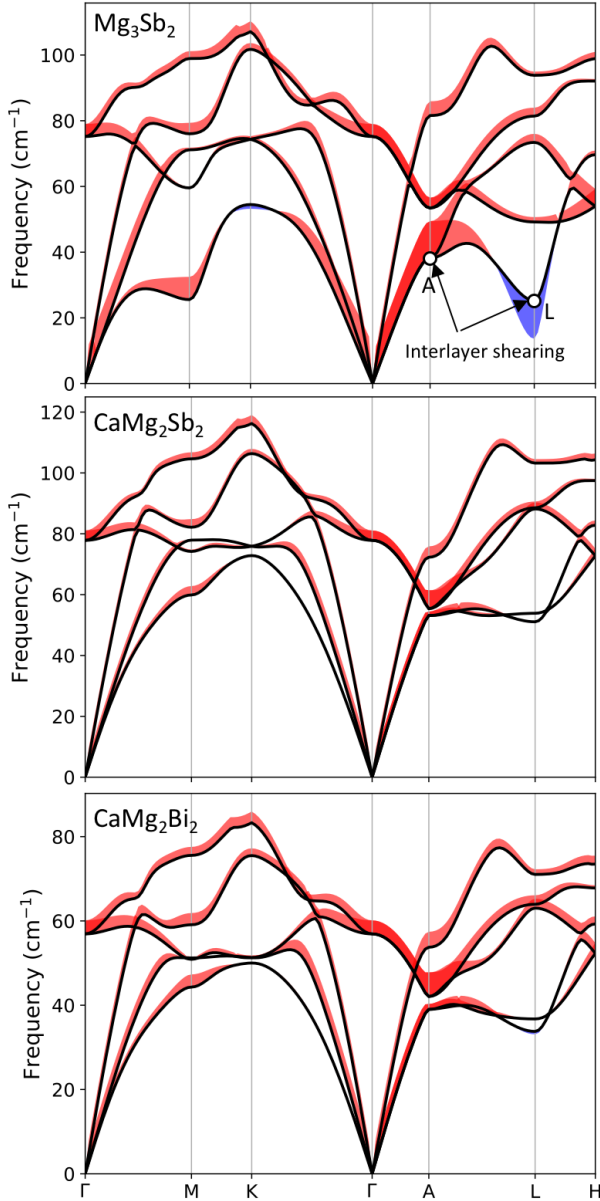


Fig. 4. The phonon dispersions of Mg_3Sb_2 , $CaMg_2Sb_2$ and $CaMg_2Bi_2$ in the low frequency regime. The mode Grüneisen parameters, γ_i , are shown through the thickness of the bands, with red and blue representing positive and negative values of γ_i , respectively.

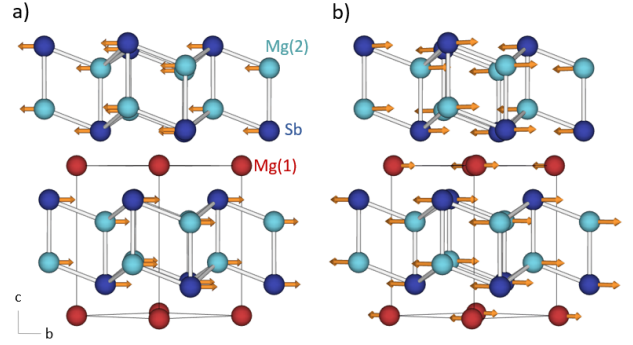


Fig. 5. Structure of Mg_3Sb_2 showing the atomic displacement corresponding to the transverse acoustic phonon modes a) at the A-point (large positive γ_i) and b) at the L-point (large negative γ_i). The corresponding modes are marked on the phonon dispersion in Figure 4.

B. *Ab initio* phonon calculations

To date, the calculated phonon density of states (DOS) and dispersion relations have only been reported for a small handful of compounds with the $CaAl_2Si_2$ structure type [52], [56]. The atom-projected DOS shown for Mg_3Sb_2 , $CaMg_2Sb_2$, and $CaMg_2Bi_2$ in Figure 3, are consistent with previous reports, which show sharply segmented frequency regimes. The anion displacement ($P_n = Sb$ or Bi) dominates at low frequencies, cation displacement is responsible for the mid-frequency modes, and the $M=Mg$ site dominates the highest frequency range. In the case of Mg_3Sb_2 , the partitioning of the two Mg sites reflects very significant differences in local bonding environment. From the lower phonon frequencies of the octahedrally-coordinated $Mg(1)$, we can infer that the $Mg(1)$ -Sb bonds are much softer than the $Mg(2)$ -Sb bonds. In fact, $Mg(1)$ occupies a similar frequency range to that Ca, showing that its bonding environment is more like that of Ca than that of $Mg(2)$.

Acoustic phonons tend to have an out-sized influence on thermal transport due to the strong frequency dependence of Umklapp ($\tau \propto 1/\omega^2$) and point defect scattering ($\tau \propto 1/\omega^4$) [59], [58], which leads to long mean free paths for low frequency phonons. The acoustic branches also tend to have higher group velocities than the optical branches, which further amplifies their relative contribution to κ_L . Any mechanism that preferentially slows or scatters acoustic phonons, therefore, can have an enormous impact on κ_L . Given that the acoustic

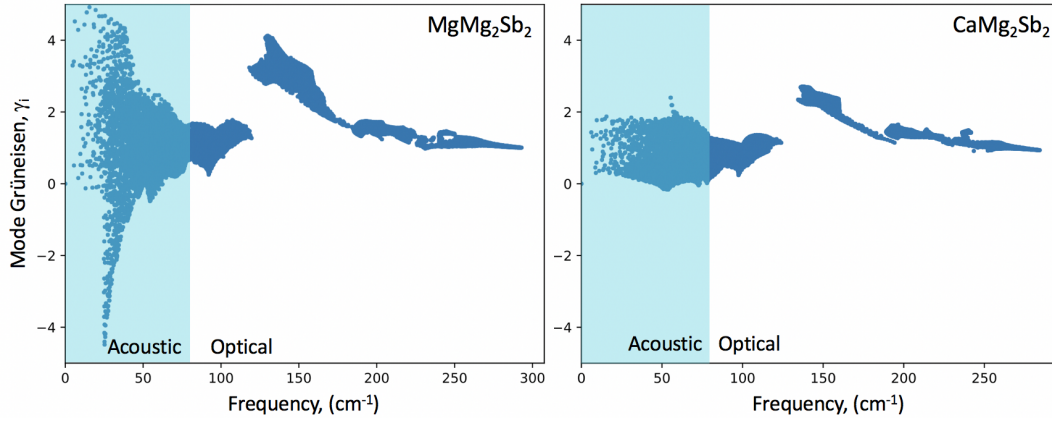


Fig. 6. The mode Grüneisen parameters as a function of frequency highlight the impact that the cation site (Mg versus Ca) has on the low frequency, acoustic phonons. In contrast, optical phonons are not strongly impacted. Data for CaMg_2Bi_2 , which behaves similarly to CaMg_2Sb_2 , is shown in the supplemental.

phonons are dominated by displacement of the anions (Figure 3), it is not immediately clear why the cation species (Mg or Ca) would greatly impact the phonon transport. Further, the average phonon group velocities at high frequencies and the Debye frequency of Mg_3Sb_2 do not appear significantly different from CaMg_2Sb_2 . We can therefore rule out differences in the phonon group velocity as the *primary* origin of the low lattice thermal conductivity in Mg_3Sb_2 .

The major differences between CaMg_2Sb_2 and Mg_3Sb_2 first become clear when we consider the phonon dispersion relations and their dependence on unit cell volume. The phonon dispersions are shown in Figure 4 in the low frequency range only, as these show the greatest change with respect to composition (the full dispersions are shown in the S.I. Figure 1). The magnitude and sign of the mode Grüneisen parameters ($\gamma_i = -\frac{V}{\omega_i} \frac{\delta\omega_i}{\delta V}$, where V is volume and ω_i is the mode frequency), are represented by the thickness and color of the dispersion curves. Since the values are all scaled with a common factor, the curve thickness is representative of the relative values of the Grüneisen parameter.

We note that the predicted slope (i.e., velocity) and volume-dependence of the longitudinal acoustic branches are similar in CaMg_2Sb_2 and Mg_3Sb_2 . In contrast, the transverse phonon modes are much softer (lower velocity) and have a stronger volume dependence in Mg_3Sb_2 . The mode Grüneisen parameters of the transverse phonons in Mg_3Sb_2 are particularly large at the Brillouin zone edge at the

A -, L -, and M -point. Those modes with the largest magnitude of γ_i involve the shearing displacement of adjacent anionic slabs in the structure. This is illustrated in Figure 5, which shows snapshots of the displacement in the Mg_3Sb_2 structure for transverse acoustic phonons at the A -point (largest positive γ_i) and at the L -point (largest negative γ_i).

By averaging the values of γ_i over all modes, weighted by the heat capacity, we can estimate bulk Grüneisen parameters of $\gamma=1.83$ and $\gamma=1.44$ in Mg_3Sb_2 and CaMg_2Sb_2 , respectively. However, as illustrated in Figure 6, which shows the mode Grüneisen parameters as a function of frequency, the highest mode Grüneisen parameters in Mg_3Sb_2 are concentrated in the acoustic frequency range (highlighted in blue), which implies that they will have a large impact on thermal transport. We note also, that the values of γ_i in the optical frequency range from 120 to 150 cm^{-1} are higher in Mg_3Sb_2 than in CaMg_2Sb_2 . These phonon modes involve almost exclusively the displacement of the cation ($\text{Mg}(1)$ or Ca), further indication of unstable $\text{Mg}(1)$ - Sb interlayer bonding. Results for CaMg_2Bi_2 , shown in the S.I. Figure 2, are similar to CaMg_2Sb_2 .

C. Experimental elastic properties and thermal expansion

The speed of sound and the elastic moduli are determined solely by the slope of the acoustic branches of the phonon dispersion at the Γ -point. Thus, measuring the high-temperature elasticity

offers a window into the behavior of the acoustic phonons near the Γ -point as a function of both temperature and unit cell volume, and can be used to evaluate the anharmonicity of these critical phonons. In the present study, resonant ultrasound spectroscopy (RUS) was used to obtain the elastic moduli, C_{11} and C_{44} , of polycrystalline AMg_2Pn_2 samples ($A=Mg, Ca, Yb$, and $Pn=Sb, Bi$) as a function of temperature, from which we obtain the shear and bulk moduli (G and K , respectively) and the transverse and longitudinal speed of sound (v_T and v_L , respectively). The details of the equations applied are listed in the S.I section 1. This method provides an accurate and non-destructive approach that has been used to study high-temperature elastic behavior of various classes of materials [32], [1]. Note that the elastic moduli and sound velocities obtained from polycrystalline samples represent an average over all crystallographic directions.

The elastic moduli of solids tend to become softer with increasing bond length [64]. Within compounds in the same structural pattern, if the unit cell volume increases, the elastic moduli are therefore expected to decrease. As shown in Figure 8, this trend is observed in AMg_2Pn_2 compounds in both the experimental ($A=Mg, Ca, Yb$ and $Pn=Sb, Bi$) and computational elastic moduli ($A=Mg, Ca, Sr, Ba$ and $Pn=P, As, Sb, Bi$) obtained from the Materials Project [8]. The only significant outliers are the shear moduli of Mg_3Sb_2 and Mg_3Bi_2 , which are much softer than compounds with similar unit cell volume. This suggests that the $Mg(1)$ - Sb bonds connecting neighboring layers are quite weak compared with other AMg_2Pn_2 compounds. Note that we omitted the computed elastic moduli of rare-earth-containing compounds due to poor agreement with experiment. These values are included in the S.I. table 1, however. Soft shear moduli are often seen in layered compounds with weak van der Waal bonds [22], [16], [63] and in the extreme case, disappearing shear modes at high temperature have been associated with liquid-like behavior [30]. In layered Zintl phases, however, the ionic bonds between adjacent anionic layers are expected to be strong, particularly in comparison with van der Waals solids. This is reflected by the relatively isotropic phonon dis-

persions of $CaMg_2Sb_2$ and $CaMg_2Bi_2$. The soft shear moduli in Mg_3Sb_2 and Mg_3Bi_2 , in contrast is anomalous.

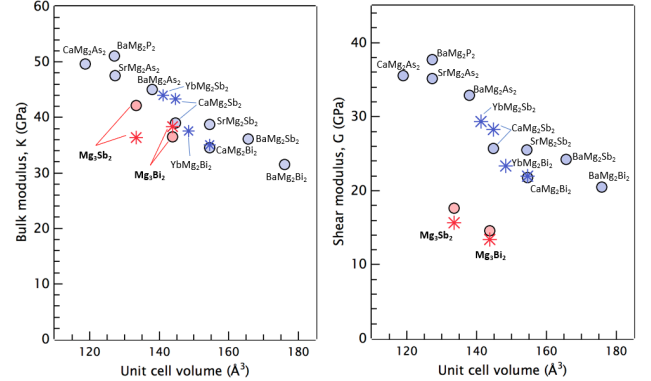


Fig. 7. Experimental (asterisk) and computed (circles) elastic moduli of AMg_2Pn_2 compounds tend to decrease as a function of increasing unit cell volume and bond length. The anomalously low shear moduli of Mg_3Sb_2 and Mg_3Bi_2 are significant, suggesting soft bonding unique to these two binary compounds [9].

Fig. 8 a) and b) shows the experimental temperature-dependence of the Young's and shear moduli of AMg_2Pn_2 samples with $A=Mg, Ca, Yb$ and $Pn=Sb, Bi$. We have included the high-temperature Young's modulus of $Si_{0.8}Ge_{0.2}$ [32], $PbTe$ [44] and $SnTe$ [45] for comparison. In a purely harmonic model, the elastic moduli do not soften with increasing temperature. The degree to which a material deviates from this behavior can be used to quantify the degree of anharmonicity. $Si_{0.8}Ge_{0.2}$ softens slowly with respect to temperature, consistent with its small Grüneisen parameter ($\gamma=1.06$ in pure Si [36]), while $PbTe$ and $SnTe$, which are known to be highly anharmonic, soften more rapidly ($\gamma=2.1$ in $PbTe$ [44]). Over the measured temperature range, we find that the elastic moduli of Mg_3Bi_2 and Mg_3Sb_2 soften by $\sim 25\%$, in comparison to a $\sim 5\%$ decrease for $CaMg_2Pn_2$ and $YbMg_2Pn_2$ samples. The rapid rate of softening of the elastic moduli with increasing temperature ($\partial G/\partial T$ and $\partial Y/\partial T$) compared even with $PbTe$ and $SnTe$, provides direct evidence of the high anharmonicity in the acoustic branches of these compounds.

The thermal expansion coefficients (α) of the compounds in this study were measured using high temperature X-ray diffraction (shown in the S.I.). For comparison, the computed thermal expansion as well as the temperature-dependent elastic mod-

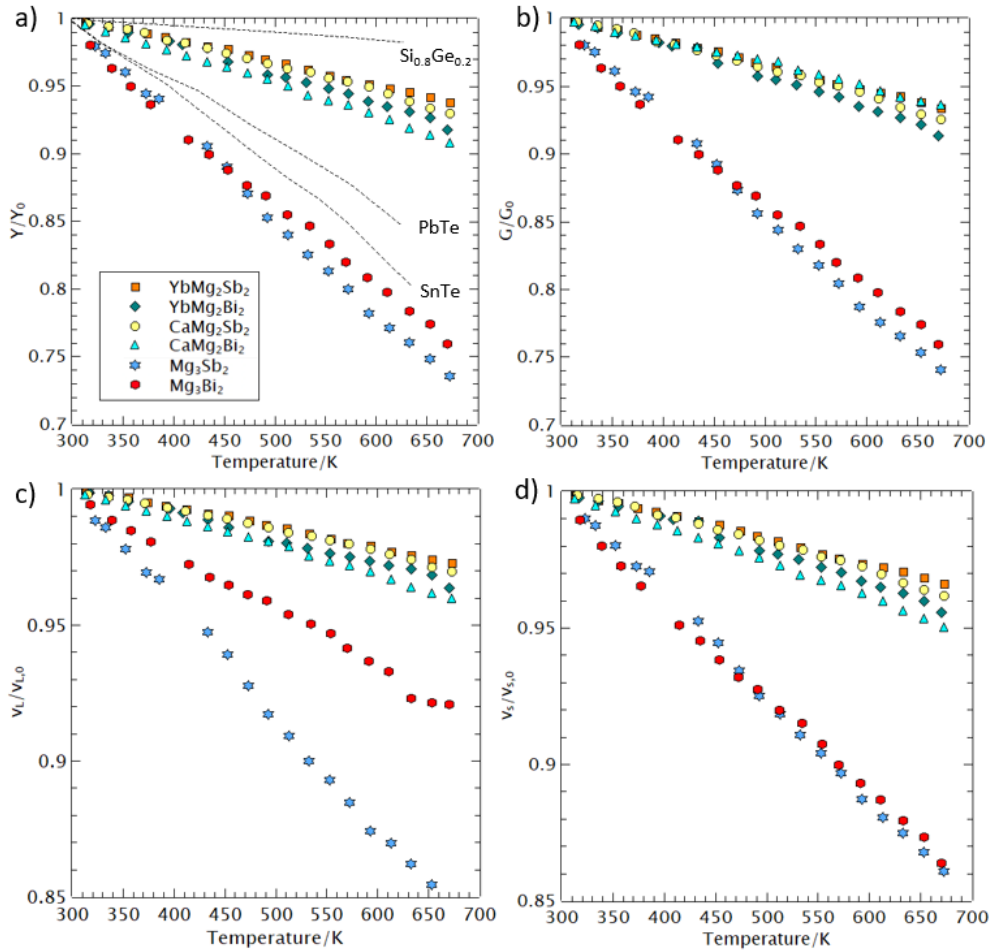


Fig. 8. Temperature-dependent a) Young’s modulus, b) shear modulus, and c) longitudinal and d) transverse speed of sound measured using resonant ultrasound spectroscopy. Quantities were normalized to the room temperature value. Data for $\text{Si}_{0.8}\text{Ge}_{0.2}$, PbTe , and SnTe are from Ref. [44], [45], [32].

uli of Mg_3Sb_2 , CaMg_2Sb_2 , and CaMg_2Bi_2 are shown in the S.I Figure 3. Experimentally, we find that Mg_3Sb_2 and Mg_3Bi_2 have higher thermal expansion than other AMg_2Pn_2 ($A=\text{Ca}$, Yb and $\text{Pn}=\text{Sb}$, Bi) compounds, as expected given their higher Grüneisen parameters. However, the contrast between the measured values of α in the binary versus the ternary variants is much less impressive than the difference in the temperature-dependence of their elastic moduli, $\partial G/\partial T$ and $\partial Y/\partial T$. This likely reflects the stronger dependence of the $\partial G/\partial T$ and $\partial Y/\partial T$ on the acoustic branches, which, as shown above, are more anharmonic than the optical branches. We thus regard the measurement of $\partial G/\partial T$ and $\partial Y/\partial T$ as an indicator of the “acoustic Grüneisen parameter”.

D. Breaking Pauling’s radius ratio rule

Among the AMg_2Pn_2 compounds considered in this study, soft shear moduli and high anharmonicity appears to be unique to the binary compounds Mg_3Sb_2 and Mg_3Bi_2 , despite their relatively low densities. This begs the question of what is so special about the presence of $\text{Mg}(1)$ on the octahedrally-coordinated cation site? One immediately apparent factor is the size of Mg , which is smaller than any other cation that can occupy the octahedral site (e.g., Ca , Yb , Sr , Eu , and Ba). Several studies have investigated the effect of the cation size in AM_2X_2 compounds [24], [26], finding that the ThCr_2Si_2 structure type (in which the cation is 8-fold coordinated) is preferred over the CaAl_2Si_2 structure type in compounds with large cations such as Ba , K Rb . Here, we

consider the opposite extreme: cations that are too small. In the sphere packing model proposed by Pauling for ionic solids, the smallest stable cation to anion radius for octahedral coordination is given by $r_{\text{cation}}:r_{\text{anion}}=0.414$ [40]. Figure 9 shows the estimated $r_{\text{cation}}:r_{\text{anion}}$ for AMg_2Pn_2 compounds. We employed ionic radii for the cations assuming a valence of 2+ and a coordination number of 6 from ref [11], [47]. The anionic radii were estimated empirically by taking the average $A-X$ distance in the $CaAl_2Si_2$ structure and subtracting the corresponding cation radii, yielding $r_P = 1.93$ Å, $r_{As} = 2.07$ Å, $r_{Sb} = 2.23$ Å, and $r_{Bi} = 2.29$ Å. Using this approach, compounds with $A=Mg$ have $r_{\text{cation}}:r_{\text{anion}}$ below the stability limit, while compounds with larger cations are stable in a six-fold coordinated environment.

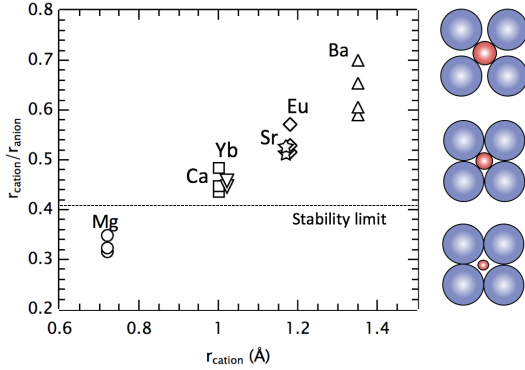


Fig. 9. For octahedral coordination (CN=6), Pauling’s radius ratio rules predict a minimum stability limit of $r_{\text{cation}}:r_{\text{anion}} = 0.414$. For Ca, Sr, Eu, and Yb, this rule is satisfied. In contrast, the Mg cation is too small, which leads to a distorted octahedral environment and may be responsible for weak, anharmonic interlayer bonding.

It is arguable whether or not the use of the ionic A radii is appropriate for this analysis, especially given the relatively small difference in electronegativity between Mg and Sb. A comparison of the Born effective charges calculated for the Mg_3Sb_2 , $CaMg_2Sb_2$ and $CaMg_2Bi_2$ (shown in the S.I. Table 3) would suggest that $Mg(1)$ -Sb bonds are more covalent than Ca-Sb bonds. If the $Mg(1)$ effectively donates fewer than two valence electrons, its effective radius would also be larger, perhaps pushing the $r_{\text{cation}}:r_{\text{anion}}$ ratio above the predicted stability limit. There are additional factors, however, supporting the view that Mg is unstable in the octahedral site, including the strong distortion of the octahedral environment around Mg and the

presence of a phase transition at high temperatures. The $MgPn_6$ octahedra in Mg_3Sb_2 and Mg_3Bi_2 exhibit bond angle variances of 26.53° and 36.01° respectively. In comparison, the octahedral bond angle variance in $CaMg_2Sb_2$ and $CaMg_2Bi_2$ is only 1.77° and 5.04° . Further, Mg_3Sb_2 and Mg_3Bi_2 are the only AMg_2Pn_2 compounds reported to undergo a structural phase transition at high temperature, which occurs at $\sim 900^\circ C$ and $\sim 700^\circ C$ respectively [46]. In the cubic, high-temperature structure (Sc_2O_3 structure type, space group $Ia\bar{3}$), Mg is tetrahedrally coordinated and satisfies Pauling’s radius ratio rule.

The instability of the small $Mg(1)$ cations in the octahedral A site of the $CaAl_2Si_2$ structure is likely responsible for both the unusually soft shear moduli and the highly anharmonic transverse phonon modes in Mg_3Sb_2 and Mg_3Bi_2 . The weakening of ionic interlayer bonds would be expected to decrease the shear elastic moduli (Figure 8, and thus reduce the speed of sound relative to stiff compounds. As shown in Figure 2b), this effect alone is insufficient to explain the factor of three reduction in κ_L of Mg_3Sb_2 compared with $CaMg_2Sb_2$. It is likely the undersized $Mg(1)$ also has a destabilizing effect, leading to the observed high-temperature phase transition and also to the exceptionally high anharmonicity observed in low-frequency modes that are associated with shearing of adjacent layers, and in mid-frequency modes due to the motion of the $Mg(1)$ cations (see Figure 4 and Figure 5). “Giant anharmonicity” is well known to occur in the vicinity of lattice instabilities, as reported for $PbTe$, $SnSe$, $GeTe$, [20], [31], so it is not entirely surprising to see the same effect in this system as well. Above the phase transition in Mg_3Sb_2 and Mg_3Bi_2 , we would expect the elastic moduli, speed of sound, and lattice thermal conductivity to exhibit a sharp increase.

In some ways, the undersized Mg in the octahedral site of the $CaAl_2Si_2$ structure is reminiscent of the filler atoms in clathrates and skutterudites which “rattle” in their oversized cages [38], [37], [60]. In such compounds, smaller cations are also desirable, as they can lead to stronger scattering and lower lattice thermal conductivity. However, cage compounds differ from the layered system in the present study in one important regard: the

cages are formed from stiff covalent bonds that are not destabilized by undersized cations. In the case of Mg_3Sb_2 , the Sb atoms that form the "cage" around Mg have a closed shell configuration and cannot form bonds between adjacent layers. This destabilizing effect leads to highly anharmonic acoustic phonons. In contrast, a fully filler rattler site leads to a flat optical mode coming down and crossing the acoustic modes [58].

IV. CONCLUSION

Inherently low lattice thermal conductivity is typically associated with dense materials or compounds with complexity at the atomic scale or on a micro-structural level. The unusually low lattice thermal conductivity of Mg_3Sb_2 , in contrast, shows that structural instability alone is sufficient, even in a very simple structure, to cause exceptionally high phonon scattering rates and low lattice thermal conductivity. By combining ab initio phonon calculations and high-temperature elasticity measurements, we showed that both Mg_3Sb_2 and Mg_3Bi_2 are highly anharmonic, in contrast to the Ca- and Yb-containing AMg_2Pn_2 compounds investigated here. Large mode Grüneisen parameters, both negative and positive, were predicted in the acoustic branches of Mg_3Sb_2 and Mg_3Bi_2 , which are expected to have a large contribution to thermal transport. This was confirmed experimentally by the rapid decrease of the speed of sound and elastic moduli in Mg_3Sb_2 with increasing temperature, which is a direct consequence of the softening of the acoustic modes. We attribute the unique behavior of Mg_3Sb_2 and Mg_3Bi_2 to the small radii of Mg, which is undersized for the octahedral coordination with Sb. The poor fit of the Mg cation is suspected to lead to weak interlayer bonding, and thus to the observed soft shear modes, and ultimately, to the highly anharmonic behavior of the acoustic branches. These results suggest more broadly that soft shear modes resulting from undersized cations provide a potential path to low lattice thermal conductivity in ionic layered structures.

REFERENCES

[1] E. ASTM. Standard test method for dynamic youngs modulus, shear modulus, and poissons ratio by impulse excitation of vibration. *Annual Book of ASTM Standards*, 3, 1876.

[2] D. Bansal, J. Hong, C. W. Li, A. F. May, W. Porter, M. Y. Hu, D. L. Abernathy, and O. Delaire. Phonon anharmonicity and negative thermal expansion in SnSe. *Physical Review B*, 94(5):054307, 2016.

[3] S. Baroni, S. de Gironcoli, A. Dal Corso, and P. Giannozzi. Phonons and related crystal properties from density-functional perturbation theory. *Rev. Mod. Phys.*, 73:515–562, Jul 2001.

[4] A. Bhardwaj, A. Rajput, A. Shukla, J. Pulikkotil, A. Srivastava, A. Dhar, G. Gupta, S. Auluck, D. Misra, and R. Budhani. *RSC Adv.*, 3(22):8504–8516, 2013.

[5] K. Biswas, J. He, I. D. Blum, C.-I. Wu, T. P. Hogan, D. N. Seidman, V. P. Dravid, and M. G. Kanatzidis. High-performance bulk thermoelectrics with all-scale hierarchical architectures. *Nature*, 489(7416):414, 2012.

[6] J. K. Burdett and G. J. Miller. Fragment formalism in main-group solids: applications to aluminum boride (alb2), calcium aluminum silicide (caal2si2), barium-aluminum (baal4), and related materials. *Chemistry of Materials*, 2(1):12–26, 1990.

[7] S. K. Bux, J.-P. Fleurial, and R. B. Kaner. Nanostructured materials for thermoelectric applications. *Chemical Communications*, 46(44):8311–8324, 2010.

[8] G. Ceder and K. Persson. The materials project: A materials genome approach, 2010.

[9] M. De Jong, W. Chen, T. Angsten, A. Jain, R. Notestine, A. Gamst, M. Sluiter, C. K. Ande, S. Van Der Zwaag, J. J. Plata, et al. Charting the complete elastic properties of inorganic crystalline compounds. *Sci. Data*, 2:150009, 2015.

[10] O. Delaire, J. Ma, K. Marty, A. F. May, M. A. McGuire, M.-H. Du, D. J. Singh, A. Podlesnyak, G. Ehlers, M. Lumsden, et al. Giant anharmonic phonon scattering in PbTe. *Nature materials*, 10(8):614, 2011.

[11] C. Giacovazzo. Editor. fundamentals of crystallography. iucr, 1992.

[12] X. Gonze. First-principles responses of solids to atomic displacements and homogeneous electric fields: Implementation of a conjugate-gradient algorithm. *Phys. Rev. B*, 55:10337–10354, Apr 1997.

[13] X. Gonze, B. Amadon, P.-M. Anglade, J.-M. Beuken, F. Bottin, P. Boulanger, F. Bruneval, D. Caliste, R. Caracas, M. Côté, T. Deutsch, L. Genovese, P. Ghosez, M. Giantomassi, S. Goedecker, D. Hamann, P. Hermet, F. Jollet, G. Jomard, S. Leroux, M. Mancini, S. Mazevet, M. Oliveira, G. Onida, Y. Pouillon, T. Rangel, G.-M. Rignanese, D. Sangalli, R. Shaltaf, M. Torrent, M. Verstraete, G. Zerah, and J. Zwanziger. Abinit: First-principles approach to material and nanosystem properties. *Computer Physics Communications*, 180(12):2582 – 2615, 2009.

[14] X. Gonze, J.-M. Beuken, R. Caracas, F. Detraux, M. Fuchs, G.-M. Rignanese, L. Sindic, M. Verstraete, G. Zerah, F. Jollet, M. Torrent, A. Roy, M. Mikami, P. Ghosez, J.-Y. Raty, and D. Allan. First-principles computation of material properties: the {ABINIT} software project. *Computational Materials Science*, 25(3):478 – 492, 2002.

[15] X. Gonze and C. Lee. Dynamical matrices, born effective charges, dielectric permittivity tensors, and interatomic force constants from density-functional perturbation theory. *Phys. Rev. B*, 55:10355–10368, Apr 1997.

[16] M. Grimditch. Shear elastic modulus of graphite. *Journal of Physics C: Solid State Physics*, 16(5):L143, 1983.

[17] D. R. Hamann. Optimized norm-conserving vanderbilt pseudopotentials. *Phys. Rev. B*, 88:085117, Aug 2013.

[18] D. R. Hamann, X. Wu, K. M. Rabe, and D. Vanderbilt. Metric tensor formulation of strain in density-functional perturbation theory. *Phys. Rev. B*, 71(3), January 2005.

- [19] L. He, F. Liu, G. Hautier, M. J. T. Oliveira, M. A. L. Marques, F. D. Vila, J. J. Rehr, G.-M. Rignanese, and A. Zhou. Accuracy of generalized gradient approximation functionals for density-functional perturbation theory calculations. *Phys. Rev. B*, 89:064305, Feb 2014.
- [20] J. Hong and O. Delaire. Electronic Instability and Anharmonicity in SnSe. *arXiv preprint arXiv:1604.07077*, 2016.
- [21] K. Imasato, S. D. Kang, S. Ohno, and G. J. Snyder. Band engineering in Mg_3Sb_2 by alloying with Mg_3Bi_2 for enhanced thermoelectric performance. *Mater. Horizons*, 2017.
- [22] J. Jenkins, J. Rayne, and R. Ure Jr. Elastic moduli and phonon properties of Bi_2Te_3 . *Physical Review B*, 5(8):3171, 1972.
- [23] Z. Jiawei, S. Lirong, M. Georg K.H., F. Karl F.F., Z. Wenqing, S. Xun, and I. Bo B. Designing high-performance layered thermoelectric materials through orbital engineering. *Nat. Commun.*, 7:10892, 2016.
- [24] M. Khatun, S. S. Stoyko, and A. Mar. Quaternary Arsenides $\text{AM}_{1.5}\text{Tt}_{0.5}\text{As}_2$ (A= Na, K, Rb; M= Zn, Cd; Tt= Si, Ge, Sn): Size Effects in CaAl_2Si_2 - and ThCr_2Si_2 -Type Structures. *Inorganic chemistry*, 52(6):3148–3158, 2013.
- [25] P. Klemens. The scattering of low-frequency lattice waves by static imperfections. *Proceedings of the Physical Society. Section A*, 68(12):1113, 1955.
- [26] P. Klüfers and A. Mewis. AB_2X_2 -Verbindungen mit CaAl_2Si_2 -Struktur. *Z. Kristallog. Cryst. Mater.*, 169(1-4):135–148, 1984.
- [27] J. J. Kuo, S. D. Kang, K. Imasato, H. Tamaki, S. Ohno, T. Kanno, and G. J. Snyder. Grain boundary dominated charge transport in Mg_3Sb_2 -based compounds. *Energy Environ. Sci.*, 2018.
- [28] W. Lai, Y. Wang, D. T. Morelli, and X. Lu. From bonding asymmetry to anharmonic rattling in $\text{Cu}_{12}\text{Sb}_4\text{S}_{13}$ tetrahedrites: When lone-pair electrons are not so lonely. *Advanced Functional Materials*, 25(24):3648–3657, 2015.
- [29] S. Lee, K. Esfarjani, T. Luo, J. Zhou, Z. Tian, and G. Chen. Resonant bonding leads to low lattice thermal conductivity. *Nature communications*, 5:3525, 2014.
- [30] B. Li, H. Wang, Y. Kawakita, Q. Zhang, M. Feyngenson, H. Yu, D. Wu, K. Ohara, T. Kikuchi, K. Shibata, et al. Liquid-like thermal conduction in intercalated layered crystalline solids. *Nature materials*, page 1, 2018.
- [31] C. W. Li, J. Hong, A. F. May, D. Bansal, S. Chi, T. Hong, G. Ehlers, and O. Delaire. Orbital driven giant phonon anharmonicity in SnSe. *Nature Physics*, 11(12):1063, 2015.
- [32] G. Li and J. Gladden. High temperature resonant ultrasound spectroscopy: a review. *International Journal of Spectroscopy*, 2010, 2010.
- [33] G. K. Madsen and G. Santi. Anharmonic lattice dynamics in type-i clathrates from first-principles calculations. *Physical Review B*, 72(22):220301, 2005.
- [34] M. Martinez-Ripoll, A. Haase, and G. Brauer. The crystal structure of $\alpha\text{-Mg}_3\text{Sb}_2$. *Acta Cryst. Section B: Structural Crystall. and Crystal Chem.*, 30(8):2006–2009, 1974.
- [35] H. J. Monkhorst and J. D. Pack. Special points for Brillouin-zone integrations. *Phys. Rev. B*, 13(12):5188–5192, June 1976.
- [36] D. T. Morelli and G. A. Slack. High lattice thermal conductivity solids. In *High thermal conductivity materials*, pages 37–68. Springer, 2006.
- [37] G. Nolas, D. Morelli, and T. M. Tritt. Skutterudites: A phonon-glass-electron crystal approach to advanced thermoelectric energy conversion applications. *Annual Review of Materials Science*, 29(1):89–116, 1999.
- [38] G. S. Nolas, G. A. Slack, and S. B. Schujman. Semiconductor clathrates: A phonon glass electron crystal material with potential for thermoelectric applications. In *Semiconductors and semimetals*, volume 69, pages 255–300. Elsevier, 2001.
- [39] S. Ohno, K. Imasato, S. Anand, H. Tamaki, S. D. Kang, P. Gorai, H. K. Sato, E. S. Toberer, T. Kanno, and G. J. Snyder. Phase boundary mapping to obtain n-type Mg_3Sb_2 -based thermoelectrics. *Joule*, 2017.
- [40] L. Pauling. *The Nature of the Chemical Bond*, volume 260. Cornell university press Ithaca, NY, 1960.
- [41] W. Peng, S. Chanakian, and A. Zevalkink. *Inorg. Chem. Front.*, xx:xx, 2018.
- [42] J. P. Perdew, A. Ruzsinszky, G. I. Csonka, O. A. Vydrov, G. E. Scuseria, L. A. Constantin, X. Zhou, and K. Burke. Restoring the density-gradient expansion for exchange in solids and surfaces. *Phys. Rev. Lett.*, 100:136406, Apr 2008.
- [43] G. Petretto, X. Gonze, G. Hautier, and G.-M. Rignanese. Convergence and pitfalls of density functional perturbation theory phonons calculations from a high-throughput perspective. *Computational Materials Science*, 144:331–337, Mar. 2018.
- [44] F. Ren, E. D. Case, J. R. Sootsman, M. G. Kanatzidis, H. Kong, C. Uher, E. Lara-Curzio, and R. M. Trejo. The high-temperature elastic moduli of polycrystalline pbte measured by resonant ultrasound spectroscopy. *Acta Materialia*, 56(20):5954–5963, 2008.
- [45] R. D. Schmidt, E. D. Case, J. E. Ni, R. M. Trejo, E. Lara-Curzio, R. J. Korkosz, and M. G. Kanatzidis. High-temperature elastic moduli of thermoelectric $\text{SnTe}_{1\pm x}\text{-y SiC}$ nanoparticulate composites. *Journal of materials science*, 48(23):8244–8258, 2013.
- [46] L. Sevastyanova, O. Kravchenko, O. Gulish, V. Stupnikov, M. Leonova, and M. Zhizhin. Binary and ternary compounds in the Mg-Sb-B and Mg-Bi-B systems as catalysts for the synthesis of cubic BN. *Inorganic materials*, 42(8):863–866, 2006.
- [47] R. T. Shannon and C. T. Prewitt. Effective ionic radii in oxides and fluorides. *Acta Crystallographica Section B: Structural Crystallography and Crystal Chemistry*, 25(5):925–946, 1969.
- [48] J. Shuai, H. Geng, Y. Lan, Z. Zhu, C. Wang, Z. Liu, J. Bao, C.-W. Chu, J. Sui, and Z. Ren. *Proc. Natl. Acad. Sci. U.S.A.*, 113(29):E4125E4132, 2016.
- [49] J. Shuai, J. Mao, S. Song, Q. Zhang, G. Chen, and Z. Ren. Recent progress and future challenges on thermoelectric zintl materials. *Materials Today Physics*, 1:74–95, 2017.
- [50] J. Shuai, J. Mao, S. Song, Q. Zhu, J. Sun, Y. Wang, R. He, J. Zhou, G. Chen, D. J. Singh, et al. Tuning the carrier scattering mechanism to effectively improve the thermoelectric properties. *Energy Environ. Sci.*, 10(3):799–807, 2017.
- [51] J. Shuai, Y. Wang, H. S. Kim, Z. Liu, J. Sun, S. Chen, J. Sui, and Z. Ren. *Acta Mater.*, 93:187–193, 2015.
- [52] D. J. Singh and D. Parker. Electronic and transport properties of zintl phase AeMg_2Pn_2 , Ae= Ca, Sr, Ba, Pn= As, Sb, Bi in relation to Mg_3Sb_2 . *Journal of Applied Physics*, 114(14):143703, 2013.
- [53] G. A. Slack. The thermal conductivity of nonmetallic crystals. In *Solid state physics*, volume 34, pages 1–71. Elsevier, 1979.
- [54] L. Song, J. Zhang, and B. B. Iversen. *J. Mater. Chem.*, 5(10):4932–4939, 2017.
- [55] H. Tamaki, H. K. Sato, and T. Kanno. Isotropic Conduction Network and Defect Chemistry in $\text{Mg}^{3+\delta}\text{Sb}_2$ -Based Layered Zintl Compounds with High Thermoelectric Performance. *Advanced Materials*, 28(46):10182–10187, 2016.

- [56] J.-i. Tani, M. Takahashi, and H. Kido. Lattice dynamics and elastic properties of Mg_3As_2 and Mg_3Sb_2 compounds from first-principles calculations. *Physica B: Condensed Matter*, 405(19):4219–4225, 2010.
- [57] E. S. Toberer, C. A. Cox, S. R. Brown, T. Ikeda, A. F. May, S. M. Kauzlarich, and G. J. Snyder. Traversing the Metal-Insulator Transition in a Zintl Phase: Rational Enhancement of Thermoelectric Efficiency in $\text{Yb}_{14}\text{Mn}_{1-x}\text{Al}_x\text{Sb}_{11}$. *Advanced Functional Materials*, 18(18):2795–2800, 2008.
- [58] E. S. Toberer, A. Zevkink, and G. J. Snyder. Phonon engineering through crystal chemistry. *J. Mater. Chem.*, 21(40):15843–15852, 2011.
- [59] T. M. Tritt. *Thermal conductivity: theory, properties, and applications*. Springer Science & Business Media, 2005.
- [60] C. Uher. Skutterudites: Prospective novel thermoelectrics. In *Semiconductors and semimetals*, volume 69, pages 139–253. Elsevier, 2001.
- [61] M. van Setten, M. Giantomassi, E. Bousquet, M. Verstraete, D. Hamann, X. Gonze, and G.-M. Rignanese. The PseudoDojo : Training and grading a 85 element optimized norm-conserving pseudopotential table. *Computer Physics Communications*, 226:39–54, May 2018.
- [62] X.Gonze, F.Jollet, F. Araujo, D.Adams, B.Amadon, T.Applecourt, C.Audouze, J.-M.Beuken, J.Bieder, A.Bokhanchuk, E.Bousquet, F.Bruneval, D.Caliste, M.Cote, F.Dahm, F. Pieve, M.Delaveau, M. G. ando B.Dorado, C.Espejo, G.Geneste, L.Genovese, A.Gerossier, M.Giantomassi, Y.Gillet, D.R.Hamann, L.He, G.Jomard, J. Janssen, S. Roux, A.Levitt, A.Lherbier, F.Liu, I.Lukacevic, A.Martin, C.Martins, M.J.T.Oliveira, S.Ponce, Y.Pouillon, T.Rangel, G.-M.Rignanese, A.H.Romero, B.Rousseau, O.Rubel, A.A.Shukri, M.Stankovski, M.Torrent, M. Setten, B. Troeye, M.J.Verstraete, D.Waroquier, J.Wiktor, B.Xue, A.Zhou, and J.W.Zwanziger. Recent developments in the abinit software package. *Computer Physics Communications*, 205:106, 2016.
- [63] H. Zabel. Phonons in layered compounds. *Journal of Physics: Condensed Matter*, 13(34):7679, 2001.
- [64] W. G. Zeier. New tricks for optimizing thermoelectric materials. *Current Opinion in Green and Sustainable Chemistry*, 4:23–28, 2017.
- [65] J. Zhang, L. Song, A. Mamakhel, M. R. V. Jørgensen, and B. B. Iversen. High-performance low-cost n-type Se-doped Mg_3Sb_2 -based Zintl compounds for thermoelectric application. *Chemistry of Materials*, 29(12):5371–5383, 2017.
- [66] J. Zhang, L. Song, S. H. Pedersen, H. Yin, L. T. Hung, and B. B. Iversen. Discovery of high-performance low-cost n-type Mg_3Sb_2 -based thermoelectric materials with multi-valley conduction bands. *Nat. Comm.*, 8:13901, 2017.